Received: 5 February 2021 | Revised: 7 April 2021 | Accepted: 8 April 2021

DOI: 10.1111/jnc.15365

ORIGINAL ARTICLE

Journal of Neurochemistry JNC The Official Journal of the International Society for Neurochemistry WILEY

Neuronally expressed a-series gangliosides are sufficient to prevent the lethal age-dependent phenotype in GM3-only expressing mice

Rhona McGonigal[1] | Jennifer A. Barrie[1] | Denggao Yao[1] | Lauren E. Black[2] | Mark McLaughlin[2] | Hugh J. Willison[1]

[1]Institute of Infection, Immunity & Inflammation, University of Glasgow, Glasgow, United Kingdom of Great Britain and Northern Ireland

[2]School of Veterinary Medicine, University of Glasgow, Glasgow, United Kingdom of Great Britain and Northern Ireland

Correspondence
Rhona McGonigal, Institute of Infection, Immunity & Inflammation, SGDB, B330, 120 University Place, University of Glasgow, Glasgow G12 8TA, United Kingdom of Great Britain and Northern Ireland.
Email: Rhona.Mcgonigal@glasgow.ac.uk

Funding information
Wellcome Trust, Grant/Award Number: 092805 and 202789; University of Glasgow Vet Fund

Abstract

Gangliosides are expressed on plasma membranes throughout the body and enriched in the nervous system. A critical role for complex *a*- and *b-series* gangliosides in central and peripheral nervous system ageing has been established through transgenic manipulation of enzymes in ganglioside biosynthesis. Disrupting GalNAc-transferase (GalNAc-T), thus eliminating all *a*- and *b-series* complex gangliosides (with consequent over-expression of GM3 and GD3) leads to an age-dependent neurodegeneration. Mice that express only GM3 ganglioside (double knockout produced by crossing *GalNAc-T*$^{-/-}$ and *GD3 synthase*$^{-/-}$ mice, *Dbl KO*) display markedly accelerated neurodegeneration with reduced survival. Degenerating axons and disrupted node of Ranvier architecture are key features of complex ganglioside-deficient mice. Previously, we have shown that reintroduction of both *a*- and *b-series* gangliosides into neurons on a global *GalNAcT*$^{-/-}$ background is sufficient to rescue this age-dependent neurodegenerative phenotype. To determine the relative roles of *a- and b-series* gangliosides in this rescue paradigm, we herein reintroduced GalNAc-T into neurons of *Dbl KO* mice, thereby reconstituting *a-series* but not *b-series* complex gangliosides. We assessed survival, axon degeneration, axo–glial integrity, inflammatory markers and lipid-raft formation in these *Rescue* mice compared to wild-type and *Dbl KO* mice. We found that this neuronal reconstitution of *a-series* complex gangliosides abrogated the adult lethal phenotype in *Dbl KO* mice, and partially attenuated the neurodegenerative features. This suggests that whilst neuronal expression of *a-series* gangliosides is critical for survival during ageing, it is not entirely sufficient to restore complete nervous system integrity in the absence of either *b-series* or glial *a-series* gangliosides.

KEYWORDS

a-series gangliosides, GM3, nervous system integrity, transgenic mice

Abbreviations: BCA, bicinchoninic acid; Caspr, contactin-associated protein; CST, cerebroside sulfotransferase; Galc, galactocerebroside; GalNAc-T, B4galnt1/β-1,4-*N*-acetylegalactosaminyltransferase 1; GD3s, α-2,8-sialyltransferase; KO, knockout; Kv, voltage-gated potassium channel; MAG, myelin-associated glycoprotein; Nav, voltage-gated sodium channel; NF, neurofascin; NF-H, anti-phosphorylated neurofilament-H antibody; NoR, node of Ranvier; PLP, proteolipid protein; pNFasc, pan-neurofascin.

1 | INTRODUCTION

Gangliosides are a family of sialic acid-containing glycosphingolipids expressed on the external leaflet of most eukaryotic cell plasma membranes and highly enriched in nervous tissue (Yu et al., 2011). Whilst neural development and differentiation were the major functions historically attributed to gangliosides, more recently an essential role in nervous system maintenance and stability has been reported (Sheikh, Sun, et al., 1999; Susuki, Baba, et al., 2007; Takamiya et al., 1996). GM3 is the first simple ganglioside synthesised by the addition of α2,3-linked sialic acid to a lactosylceramide core (Figure 2a). GM3 is then modified by the β1,4-N-acetylgalactosaminyltransferase 1 enzyme (B4galnt1 or GalNAc-T) or by the α-2,8-sialyltransferase (GD3 synthase, GD3s) enzyme to produce *a-series* or *b-series* gangliosides respectively. It is GM1 & GD1a from the *a-series*, and GD1b & GT1b from the *b-series* that form the majority of the gangliosides expressed in the normal nervous system. Transgenic manipulations of the key enzymes that disrupt the ganglioside biosynthesis pathway have been used to elucidate the physiological function of gangliosides and have by and large demonstrated a high degree of functional redundancy. Despite this redundancy, the increasing loss of heterogeneity in the overall complement of gangliosides in general enhances the neurodegenerative phenotype and mortality of mice, suggesting complex and subtle roles for different gangliosides in fine-tuning the nervous system over the lifespan. As gangliosides are synthesised by step-wise addition of hexose sugars to the elongating glycan core by multiple enzymes, block of one biosynthetic step leads to overflow into alternative biosynthetic steps, leading to complex changes in ganglioside profiles that are as yet poorly understood. At the least severe end of the spectrum, *GD3s*$^{-/-}$ mice that lack *b-series* complex gangliosides and thus over-express *a-series* gangliosides have a normal lifespan with no overt neurodegenerative phenotype. However, these mice exhibit a regenerative deficiency suggesting a role for *b-series* gangliosides in neural repair (Okada et al., 2002). *GalNAc-T*$^{-/-}$ mice that express no complex gangliosides whilst over-accumulating the simple precursor gangliosides GM2, GD3 and 9-O-acetyl GD3 have a near-normal lifespan but develop age-dependent demyelination, axonal degeneration and a loss of axo–glial integrity at the node of Ranvier (NoR) (Sheikh, Sun, et al., 1999; Susuki, Baba, et al., 2007). Cross-breeding the *GD3s*$^{-/-}$ and *GalNAc-T*$^{-/-}$ transgenic strains results in double *a-* and *b-series* null mice with a consequent accumulation of GM3 (GM3-only, *Dbl knockout [KO]* mice, Table 1). These mice have a severe post-natal neurodevelopmental phenotype with seizures, paralysis and early death. Notably, the severity of the *Dbl KO* phenotype appears to differ among research groups, presumably owing to subtle differences acquired in the background C57BL/6 mouse strains on which the mice are maintained (Inoue et al., 2002; Kawai et al., 2001). Mice lacking all gangliosides including GM3 develop a severe and lethal phenotype following weaning (Yamashita et al., 2005). In the total absence of gangliosides, there is a loss of transverse bands at the paranodal junction (Yamashita et al., 2005), but the effect on the organisation at the NoR has yet to be described with GM3-only ganglioside expression. Mice double null for galactocerebroside (GalC) and myelin-associated glycoprotein (MAG), *GalC*$^{-/-}$ × *MAG*$^{-/-}$ (Marcus et al., 2002), or gangliosides and sulfatides, *GalNAc-T*$^{-/-}$ × *CST*$^{-/-}$ (McGonigal et al., 2019), have a severe phenotype with rapid and profound neurodegeneration resulting in death soon after weaning, suggesting the necessity for gangliosides, galactolipids and their interactive ligands in axo–glial homeostasis. Humans with mutations in ganglioside biosynthesis enzymes GM3s or GalNAc-T similarly develop neurodevelopmental and neurodegenerative syndromes that fall into the severe end of the spectrum compared to mice, emphasising the importance of complex ganglioside expression beyond ageing, at least in man (Boukhris et al., 2013; Simpson et al., 2004).

Complex gangliosides are abundantly expressed in the brain and peripheral nerves (Ogawa-Goto & Abe, 1998; Svennerholm et al., 1994; Takamiya et al., 1996; Vajn et al., 2013). The *a-series* complex gangliosides, GM1 and GD1a exhibit the greatest enrichment in peripheral nerve axons and localisation at NoR (McGonigal et al., 2010; Sheikh et al., 1999; Susuki, Baba, et al., 2007). This correlates with the increased incidence of autoantibodies against these gangliosides in the axonal variant of the autoimmune peripheral neuropathy Guillain–Barré syndrome (Willison & Yuki, 2002), where the motor axons are targeted, especially at the NoR. Nodal disruption has been found in both axonal Guillain–Barré syndrome animal models and from human tissue (Griffin et al., 1996; McGonigal et al., 2010; Susuki, Rasband, et al., 2007), signifying a structural role for gangliosides at this highly specialised site. It has been proposed that gangliosides in lipid rafts promote axo–glial integrity through stabilisation of the key contactin-associated

	Wild type	*GD3s*$^{-/-}$ × *GalNAcT*$^{-/-}$	*GD3s*$^{-/-}$ × *GalNAcT*$^{-/-}$ *Tg(neuronal)*
Abbreviated nomenclature	WT	*Dbl KO*	*Rescue*
GalNAc transferase expressed globally	✓	✗	✗
GD3 synthase expressed globally	✓	✗	✗
a-series ganglioside expression in neurons	✓	✗	✓
b-series ganglioside expression in neurons	✓	✗	✗
GM3 over-expression, globally	✗	✓	✓

TABLE 1 Comparison of ganglioside synthesising enzyme and lipid expression profiles among the three mouse genotypes used in this study

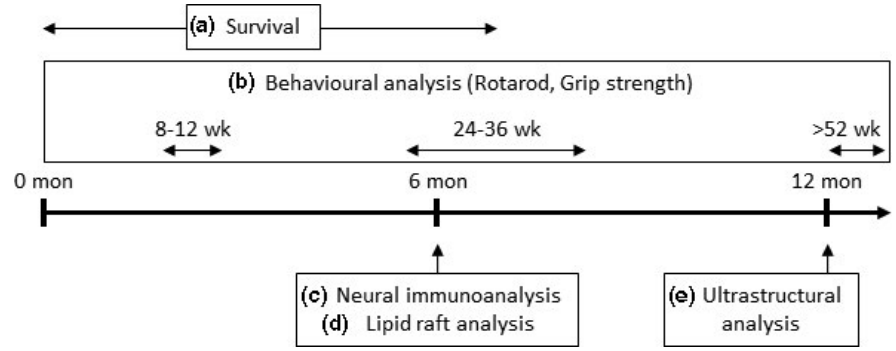

FIGURE 1 Experimental flow diagram. (a) WT $n = 146$, *Dbl KOn* = 43, *Rescuen* = 48. (b) Grip strength: WT $n = 8$ (8–12 weeks), $n = 10$ (24–36 weeks), $n = 11$ (>52 weeks); *Dbl KOn* = 5 (8–12 weeks), $n = 13$ (24–36 weeks) $n = 7$ (>52 weeks); *Rescuen* = 7 (8–12 weeks) $n = 7$ (24–36 weeks) $n = 10$ (>52 weeks). Rotarod: WT $n = 8$ (8–12 weeks), $n = 10$ (24–36 weeks), $n = 11$ (>52 weeks); *Dbl KOn* = 5 (8–12 weeks), $n = 13$ (24–36 weeks), $n = 7$ (>52 weeks); *Rescuen* = 7 (8–12 weeks), $n = 7$ (24–36 weeks), $n = 10$ (>52 weeks). (c) $n = 3$–4 per genotype. (d) $n = 3$ per genotype. (e) $n = 3$ per genotype

protein (Caspr)/neurofascin 155 (NF155) adhesion molecule complex at the paranode (Sheikh, Sun, et al., 1999; Susuki, Baba, et al., 2007), and additionally are an axonal ligand for glial MAG (Collins et al., 1997; Schnaar & Lopez, 2009; Vinson et al., 2001). An intact paranodal axo–glial junction is essential for propagation of action potentials by precluding current leakage at the NoR (Charles et al., 2002). GM1 ganglioside, in particular, has long been considered a key component of rafts and indeed the GM1 ligand, cholera-toxin B subunit, is widely used as a lipid raft marker (Merritt et al., 1994). In addition, a role for gangliosides in anchoring complement regulatory proteins in lipid rafts has been proposed as their absence may account for the up-regulation of neuroinflammatory markers in the *Dbl* KO mice resulting in inflammation and neurodegeneration (Ohmi et al., 2009).

Recently, we have reported that reintroducing complex *a*- and *b-series* gangliosides specifically into neurons of global complex ganglioside deficient mice is sufficient to nearly normalise nervous system dysfunction and pathology (Yao et al., 2014). Notably, the same restorative effect was not attained by ganglioside reintroduction into glia, underscoring the functional importance of neuronally located complex gangliosides. *GD3s*$^{-/-}$ mice lacking *b-series* gangliosides are considered to develop and age normally, and thus it might be argued that *a-series* gangliosides alone are the critical complex ganglioside constituents required for normal neural development and maintenance. However, these mice do display subtle abnormalities in nodal integrity and regeneration (Okada et al., 2002; Susuki, Baba, et al., 2007). In addition, in the absence of sulfatide, which is highly expressed on the glial membrane, we have previously shown that *a-series* gangliosides alone are insufficient to abrogate the lethal phenotype in *GD3s*$^{-/-}$ × *CST*$^{-/-}$ mice, suggesting *b-series* gangliosides are functionally important (McGonigal et al., 2019). To interrogate this further herein, we expressed *a-series* gangliosides selectively in neurons of GM3-only mice in the absence of *b-series* gangliosides to explore their critical role in more detail. Whilst reintroduction of *a-series* gangliosides in neurons largely restored survival and behavioural phenotype of GM3-only mice, this was insufficient to completely attenuate axon degeneration or nodal disruption, suggesting the requirement for glial, and/or *b-series* ganglioside expression for normal nervous system function and integrity.

2 | METHODS

2.1 | Mice

Wild type, *GD3s*$^{-/-}$ × *GalNAc-T*$^{-/-}$ and *GD3s*$^{-/-}$ × *GalNAc-T*$^{-/-}$-*Tg(neuronal)* were used: for simplicity, these genotypes will henceforth be abbreviated to WT, *Dbl KO* and *Rescue* respectively. Original *GalNAc-T*$^{-/-}$ and *GD3s*$^{-/-}$ colonies were gifted from the Furakawa laboratory 20 years ago and maintained locally on a C57BL/6 253 background (Harlan, UK). An overview of the expression of gangliosides in each genotype used in this study is outlined in Table 1. Group number and age are described in Figure 1 and per experiment below. No randomisation was performed to allocate subjects in the study. *Dbl KO* mice were produced as previously described (Inoue et al., 2002; Kawai et al., 2001) by crossing *GD3s*$^{-/-}$ (Okada et al., 2002) and *GalNAc-T*$^{-/-}$ (Takamiya et al., 1996) mice. *Rescue* mice, with reconstituted site-specific expression of *a-series* gangliosides in neurons were produced by crossing the *GD3s*$^{-/-}$ line with the recently reported *GalNAcT*$^{-/-}$*-Tg(neuronal)* line (Yao et al., 2014). Enzyme activity assays have previously been performed in the *GalNAcT*$^{-/-}$*-Tg(neuronal)* line and found to be lower than WT mice which we attributed to a dilution effect because of the analysis of whole brain rather than exclusively neuronal tissues (Yao et al., 2014; McGonigal et al., 2016). Mice were maintained under a 12-hr light/dark cycle in controlled temperature and humidity with ad libitum access to food and water. Mice, of either sex, underwent killed by CO_2 inhalation; all housing and experimental protocols were approved by and complied with UK Home Office guidelines, conformed to University of Glasgow institutional guidelines and performed under licence P0C6B3485.

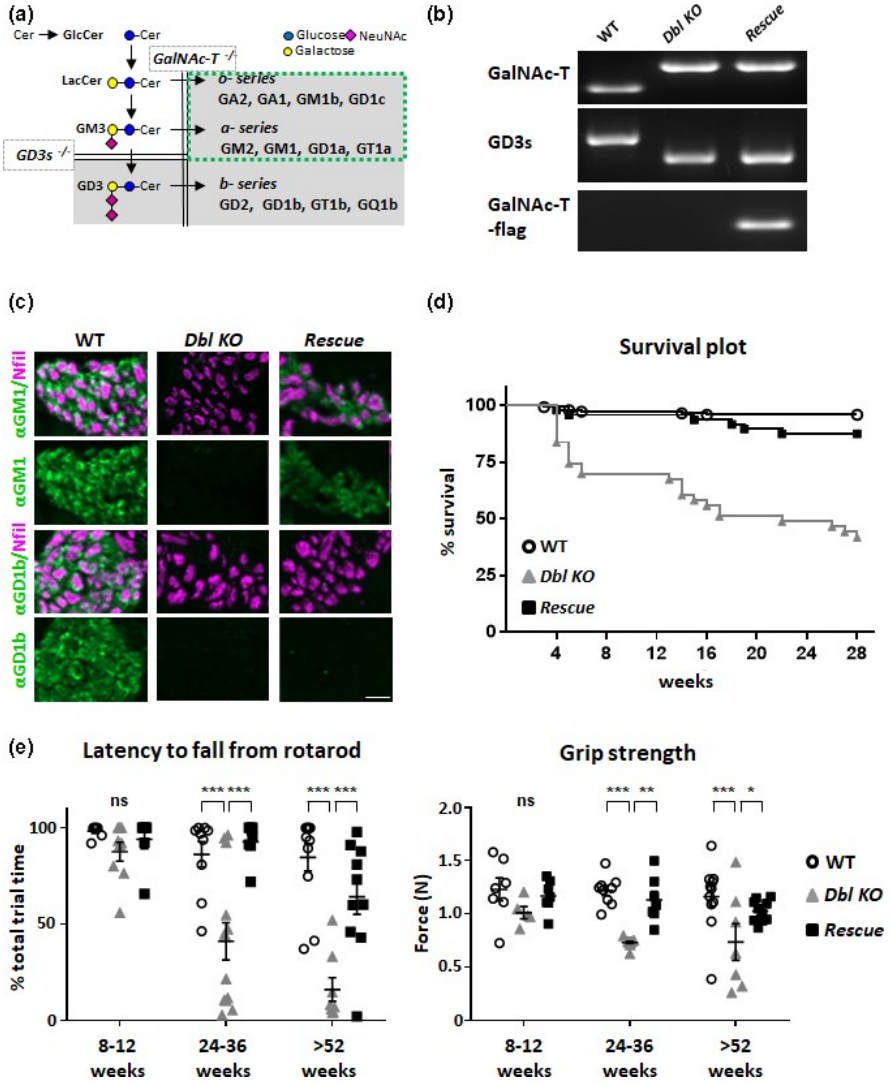

FIGURE 2 Neuronal expression of *a-series* gangliosides promotes survival and normal behaviour. (a) Ganglioside biosynthesis pathway. The GalNAc-T enzyme is necessary for generating complex gangliosides and the GD3s enzyme for production of *b-series* complex gangliosides. In mice null for both genes, *Dbl KO* mice, complex gangliosides and GD3 are not expressed (grey boxes). Constructs were generated to drive GalNAc-T expression in neurons of *Dbl KO* mice to produce the *Rescue* mouse line that have expression of *a-series* gangliosides restored neuronally (green box). (b) PCR results confirm the genotypes of the mice. The larger band and smaller band represent the disrupted GalNAc-T and GD3s genes with insert respectively. The flag identifies the reintroduction of the GalNAc-T gene into the neurons of *Rescue* mice. (c) Expression of *a-* and *b- series* gangliosides was confirmed by staining peripheral nerves with anti-GM1 and anti-GD1b monoclonal antibodies (green) respectively. Axons were identified with neurofilament (Nfil) antibody immunostaining (magenta). Scale bar =10 μm. (d) Survival plots demonstrate that *Dbl KO* mice ($n = 43$) develop normally and then show a progressive reduction in life expectancy which is halved at 18 weeks. Reconstituting *a-series* gangliosides neuronally in the *Rescue* mice ($n = 48$) results in a return to normal life expectancy similar to WT ($n = 146$). (e) Performance on the rotarod and grip strength is significantly poorer beyond 24 weeks of age in *Dbl KO* mice, and resolved to WT levels in *Rescue* mice. Rotarod: WT $n = 8$ (8–12 weeks), $n = 10$ (24–36 weeks), $n = 11$ (>52 weeks); Dbl KO $n = 5$ (8–12 weeks), $n = 13$ (24–36 weeks), $n = 7$ (>52 weeks); Rescue $n = 7$ (8–12 weeks), $n = 7$ (24–36 weeks), $n = 10$ (>52 weeks). Grip strength: WT $n = 8$ (8–12 weeks), $n = 10$ (24–36 weeks), $n = 11$ (>52 weeks); Dbl KO $n = 5$ (8–12 weeks), $n = 13$ (24–36 weeks) $n = 7$ (>52 weeks); Rescue $n = 7$ (8–12 weeks) $n = 7$ (24–36 weeks) $n = 10$ (>52 weeks). Two-way ANOVA, $^{***}p < .001$, $^{**}p < .01$ $^{*}p < .05$. Abbreviated nomenclature: Wild type (WT); *GD3s*$^{-/-}$ × *GalNAcT*$^{-/-}$ (*Dbl KO*); *GD3s*$^{-/-}$ × *GalNAc-T*$^{-/-}$*-Tg(neuronal)* (*Rescue*)

2.2 | Materials

Monoclonal antibodies used to detect complex *a-* or *b-series* gangliosides were generated by immunisation of ganglioside-deficient mice with ganglioside liposomes or ganglioside-mimicking Campylobacter jejuni lipo-oligosaccharide, as previously described (Boffey et al., 2005; Bowes et al., 2002). Anti-GM1 ganglioside antibody, DG2, and anti-GD1b antibody, MOG1, were used at 20 μg/ml in PBS. All other primary antibodies were used in a blocking solution (10% NGS +0.5% Triton X-100 in PBS) as follows: mouse anti-phosphorylated neurofilament-H antibody (NF-H, BioLegend #801602 clone SMI31; RRID:AB_2715851; 1:2000); mouse anti-pan voltage-gated sodium

channel (pNav; Sigma-Aldrich #8809; RRID:AB_477552; 1:100); rabbit anti-Caspr (gifted by Professor Peles; Weizmann Institute; 1:1,000); rabbit anti-pan neurofascin (pNFasc, gifted by Professor Brophy, University of Edinburgh; 1:1,000); mouse anti-ankyrin G (Thermo Fisher Scientific; RRID:AB_2533145; 1:100); mouse anti-MAG antibody (gifted by Professor Brophy, University of Edinburgh; 1:100); rabbit anti-voltage-gated potassium channel 1.1 (Kv1.1, Alomone Laboratories #APC-009; RRID:AB_2040144; 1:200); rabbit anti-NeuN antibody (Millipore; 1:750), rat anti-mouse F4/80 (MCAP497; Serotec; 1:500) or FITC-labelled rabbit anti-C3c (Dako; 1:300). Primary antibodies used in Western blots were rabbit anti-MAG 248 (gifted by Professor N. P. Groome, 1:10 000) and rabbit anti-pNFasc (gifted by Professor Brophy, University of Edinburgh; 1:5,000), anti-Caspr (antibodies-online.com ABIN1304571, 1:1,000); anti-Flotillin (BD Bioscience 610,821, 1:1,000); rabbit anti-proteolipid protein (PLP/DM20, raised against common C-terminal residues 271–276 and gifted by Professor N.P. Groome, 1:100,000) prepared in 5% skimmed milk powder in TBS containing 0.1% Tween-20 (T-TBS). Secondary antibodies were prepared in PBS plus 1% NGS: isotype-specific (IgG1, IgG3) Alexa Fluor 488- and 555-conjugated goat anti-mouse IgG antibodies (Invitrogen; RRID:AB_141780); Alexa Fluor 488- and Alexa Fluor 555-conjugated goat anti-rabbit antibodies (Invitrogen; RRID:AB_141761). Secondary antibodies for western blots were HRP-linked goat anti-rabbit (Dako, 1:10 000) or goat anti-mouse (Dako, 1:5,000) prepared in 5% skimmed milk/T-TBS.

2.3 | Lipid localisation

Peripheral nerves were rapidly dissected from 6-month-old mice and snap frozen. Tissue sections (10 μm) were collected onto APES-coated slides. To detect the presence of *a*- and *b-series* gangliosides, sections were treated as previously described (McGonigal et al., 2019). Representative images were captured at 40× magnification using a Zeiss AxioImager Z1 with ApoTome attachment and processed using Zeiss Zen 2 blue edition software.

2.4 | Phenotypic analysis

Mice were monitored over their natural lifespan. Survival plots over a 28-week period comparing the three genotypes were generated (WT $n = 146$; *Dbl KO* $n = 43$; *Rescue* $n = 48$). Behavioural analysis was performed in the afternoon. Grip strength (WT $n = 8$ [8–12 weeks], $n = 10$ [24–36 weeks], $n = 11$ [>52 weeks]; *Dbl KO* $n = 5$ [8–12 weeks], $n = 13$ [24–36 weeks], $n = 7$ [>52 weeks]; *Rescue* $n = 7$ [8–12 weeks], $n = 7$ [24–36 weeks], $n = 10$ [>52 weeks]) and performance on a rotarod (WT $n = 8$ [8–12 weeks], $n = 10$ [24–36 weeks], $n = 11$ [>52 weeks]; *Dbl KO* $n = 5$ [8–12 weeks], $n = 13$ [24–36 weeks], $n = 7$ [>52 weeks]; *Rescue* $n = 7$ [8–12 weeks], $n = 7$ [24–36 weeks], $n = 10$ [>52 weeks]) were assessed and statistically analysed as previously described (Yao et al., 2014). Briefly, mice were habituated to the rotarod apparatus and digital force gauge equipment (Chatillon DFIS; AMETEK) for 3 days prior to recording. Latency to fall from the rod rotating at a fixed speed of 15 rpm over a 100-s trial was recorded. Total tensile force generated from the front limbs was subtracted from the total force generated from all four limbs to calculate hindlimb grip strength. Each test was repeated three times each day over three consecutive days and the data averaged per mouse. Results were plotted as the average ±*SEM*.

2.5 | Ultrastructure

Mice (12 months, $n = 3$ per genotype) were killed by CO2 inhalation then a post-mortem transcardial perfusion with 5% glutaraldehyde/4% paraformaldehyde mixture performed before the second segment of the cervical spinal cord was removed and processed for resin embedding as previously described (Griffiths et al., 1981). Sections were cut for ultrastructural analysis. Electron micrographs from transverse sections of the ventral columns of the spinal cord at 2700x magnification were captured on a Jeol 1,200 Electron microscope. Quantification was performed as previously described (McGonigal et al., 2019). Results were plotted as the average ±*SEM*.

2.6 | Nerve protein immunoanalysis

Optic nerves, sciatic nerve and spinal cord were rapidly dissected from 6-month-old mice ($n = 3/4$ per genotype) into 4% PFA for 30 min (nerves) and overnight (cord), respectively, at 4°C. Tissue was processed and stained as previously described (McGonigal et al., 2019). Briefly, optic nerve sections and teased sciatic nerve were incubated overnight in blocking solution with the following primary antibodies: mouse anti-pNav IgG1 antibody, rabbit anti-Caspr IgG antibody, rabbit anti-Kv1.1 IgG antibody, rabbit anti-pNFasc IgG antibody or mouse anti-MAG IgG1 antibody. Spinal cord sections were incubated overnight in blocking solution with either mouse anti-NeuN antibody, rat anti-F4-80 antibody or rabbit anti-C3c-FITC antibody.

All images were captured with a Zeiss Z.1 AxioImager with ApoTome attachment or Zeiss LSM 880 microscope using Zeiss Zen 2 blue edition software. Optic nerve pNav channel cluster number and MAG intensity analysis were performed as previously described (McGonigal et al., 2019). The total length of Caspr immunostaining per node (distance between dimer outer edges minus the gap between Caspr dimers) was quantified from four 25 × 25 μm fields of view per z-stack and averaged per animal. Total length of pNFasc immunostaining was performed similarly by simply measuring the distance between dimer outer edges. For peripheral nerve node analysis, images from teased sciatic nerve were used to quantify the distance between the Caspr dimers, the distance between Kv1.1 dimers, the length of the Nav channel clusters, the length of the pNFasc domain and the total length of Caspr protein (as above) from 20 to 50 NoR per genotype. For spinal cord, images of the ventral

horn (identified by DAPI) from three non-consecutive spinal cord sections were captured. The number of NeuN or F4/80-positive cells within three 50 × 50 μm ROI was quantified. Results were plotted as the average ±*SEM*.

2.7 | Lipid raft preparation

Partitioning of proteins into lipid rafts was investigated according to the methodology of Schafer *et al*. (Schafer et al., 2004). Dissected brain tissue (6 months, $n = 3$ per genotype) was snap frozen in liquid nitrogen and stored at −80°C until required. Brain tissue was homogenised at 10 mgs/ml in homogenisation buffer (HB) composed of 0.32 M sucrose, 5 mM phosphate buffer pH 7.4, 0.5 mM PMSF, 1 mM Na-orthovanadate, 1 mM Na-pyrophosphate and a protease inhibitor cocktail (Sigma, #P8340) using a Teflon homogeniser on medium speed. Homogenates were centrifuged at 600 *g* for 10 min at 4°C and supernatants then centrifuged at 45,000 *g* for 60 min at 4°C. The membrane-enriched pellets were resuspended in HB and protein concentration determined using the BCA (bicinchoninic acid) method (Thermo Fisher Ltd). Detergent extraction was performed with 100 μg of protein in a final volume of 1 ml using an extraction buffer containing either 1% Triton X-100 (NF155, Caspr & flotillin) or 1% CHAPS (MAG and PLP), 20 mM Tris-HCl pH 8.0, 150 mM NaCl, 10 mM iodoacetamide plus the inhibitors described for HB above. Samples were rotated at 4°C for 1 hr and then centrifuged at 13,000 *g* for 60 min at 4°C. The detergent-soluble supernatant was removed and the detergent-insoluble pellet fraction resuspended in 400-μl HB and stored at −20°C until required. We will now refer to the detergent-soluble supernatant and the detergent-insoluble pellet fractions throughout the manuscript where the detergent-insoluble pellet is the lipid raft containing fraction.

Sucrose density centrifugation was performed using the Beckman SW55 rotor. Resuspended detergent-insoluble pellets were mixed with 0.8mls of 2 M sucrose, layered with 1.6 mls 1 M sucrose, then layered with 1.2 mls 0.2 M sucrose and centrifuged at 190,000 *g* for 19 hr at 4°C. Following centrifugation, 400-μl sucrose fractions were collected from top to bottom to give 10 fractions per sample. The protein content of each of the sucrose fractions obtained from the 1% Triton X-100 detergent-insoluble pellet was precipitated with 5% trichloroacetic acid (TCA) and the TCA pellets resuspended in denaturing buffer, 1% CHAPS fractions did not require precipitation. The integrity of the lipid rafts isolated using this protocol was confirmed by treating 1mg/ml of the membrane-enriched fraction with 0.2% saponin to disrupt cholesterol which is a requirement for raft formation (Cerneus et al., 1993; Rothberg et al., 1990). Samples were rotated in the presence of saponin for 30 min at 4°C followed by centrifugation at 13,000 *g* for 10 min. The detergent extraction procedure detailed above was then performed on the pelleted membrane fraction, followed by centrifugation to generate the detergent-soluble supernatant and the detergent-insoluble pellet which were stored at −20°C until required.

2.8 | Western blot analysis

Western blot was performed as described previously (McGonigal et al., 2019). In brief, samples were subjected to SDS-PAGE using BioRad criterion 4%–20% gels with MOPS buffer, transferred to nitrocellulose using the Iblot system and all blocking and antibody reactions performed using 5% skimmed milk T-TBS. Immunocomplexes formed with a HRP coupled secondary antibody were detected using the ECL method and scanned X-ray films were analysed using Image J (NIH) software.

2.9 | Experimental design and statistics

This study was an exploratory characterisation with no pre-determined exclusion criteria. A graphical flow chart of study design is shown in Figure 1. The numbers of independent animals are described in the Materials and Methods sections, and no sample calculation was performed. The experimenter performing analysis was unaware of the genotype. Statistical differences among genotypes were determined by one-way or two-way ANOVA followed by a Fisher's or Tukey's *post hoc* test using GraphPad Prism 6 software (RRID:SCR_002798). Data were not assessed for normality, ROUT tests for outliers were applied and no data points were excluded. Differences were considered significant when $p < .05$. This study was not pre-registered.

3 | RESULTS

3.1 | Neuronal a-series ganglioside expression promotes survival and a normal phenotype

Dbl KO mice that express only the simple ganglioside GM3 have a reduced lifespan and exhibit a neurodegenerative phenotype. To assess whether neuronal expression of *a-series* gangliosides is sufficient to rescue this phenotype, we generated *Rescue* mice that selectively express complex *a-series* gangliosides in neurons by backcrossing the *GD3s*$^{-/-}$ transgenic mouse strain (Inoue et al., 2002; Kawai et al., 2001; Takamiya et al., 1996) with the *GalNAcT-Tg(neuronal)* line (Yao et al., 2014). Targeted gene disruption and reintroduction in these transgenic lines were confirmed by PCR and screening for complex ganglioside expression in neural tissue by immunostaining (Figure 2). GalNAc-T and GD3s genes are disrupted by an insert, which was assessed by PCR. In Figure 2b, the larger slower migrating GalNAc-T band and smaller faster migrating GD3s bands represent appropriate disruption in both transgenic mice compared to WT. In addition, a band identifying the GalNAc-T-flag in the *Rescue* mouse strain confirms selective GalNAc-T gene expression neuronally (Figure 2b).

To demonstrate selective ganglioside expression profiles on neural membranes among the genotypes, transverse peripheral nerve sections were probed with anti-ganglioside antibodies targeting

either GM1 (*a-series*) or GD1b (*b-series*) (Figure 2c). Both anti-GM1 and -GD1b antibodies bound strongly to WT peripheral nerve bundles, confirming the presence of both *a-* and *b-series* gangliosides. Immunoreactivity was absent from nerve sections from *Dbl KO* mice, confirming specific loss of complex gangliosides from both the *a-* and *b-series*. Restoration of *a-series* and not *b-series* ganglioside expression was indicated by positive immunostaining for anti-GM1, and not anti-GD1b antibody, in *Rescue* mice. Similar results were obtained using an antibody targeting GD1a (data not shown).

Behaviourally, the *Dbl KO* mice displayed a tremor that worsened with age, and sudden death of unknown cause from 4 weeks of age onwards. Seizures were never observed, although mice were not constantly under video surveillance. A Kaplan–Meier survival plot demonstrated a significant difference among genotypes in survival rate over 28 weeks ($p < .001$, Figure 2d). Only 42% of *Dbl KO* mice survive to the end point of this study compared to a survival rate of 96% in wild-type mice. These findings are similar to those of a previous study in which only 33% *Dbl KO* mice survived at 30 weeks (Inoue et al., 2002). The presence of neuronal *a-series* gangliosides was sufficient to increase the proportion of mice surviving to 88%, which was not significantly different to WT. The age-dependent behavioural performance of mice was compared among genotypes (Figure 2e). Both rotarod performance and grip strength showed no significant difference among genotypes at 8–12 weeks. A significantly poorer performance on rotarod, determined by reduced latency to fall within the given trial period, was recorded at both 24–36 weeks and >52 weeks of age in *Dbl KO* mice compared to WT and *Rescue* mice (24–36 weeks, $p < .001$, 41.2 ± 9.7 vs. 86.2 ± 6.6%, $p < .001$ 41.2 ± 9.7 vs. 92.7 ± 4.1%; >52 weeks, $p < .001$, 16.2 ± 6.4 vs. 84.7 ± 7.1%, $p < .001$ 16.2 ± 6.4 vs. 64.2 ± 9.3%). Similarly, a significantly weaker grip strength was recorded at both 24–36 weeks and >52 weeks of age in *Dbl KO* mice compared to WT and *Rescue* mice (24–36 weeks $p < .001$, 0.73 ± 0.01 vs. 1.22 ± 0.05, $p < .01$ 0.73 ± 0.01 vs. 1.13 ± 0.08 N; >52 weeks $p < .001$, 0.74 ± 0.17 vs. 1.16 ± 0.09, $p < .05$ 0.74 ± 0.17 vs. 1.03 ± 0.03 N). The performance on rotarod and grip strength was not significantly different between WT and *Rescue* mice at any age, indicating that *a-series* ganglioside expression can restore *Dbl KO* mice to the performance level of WT.

3.2 | Neuronal expression of a-series gangliosides attenuates neurodegeneration and immune activity in Dbl KO CNS

Previous qualitative studies report that loss of some or all complex gangliosides leads to peripheral axon degeneration. Whilst this has been observed it has not previously been quantified in *Dbl KO* mice (Inoue et al., 2002). Ultrastructural analysis of the cervical spinal cord from 12-month-old *Dbl KO* animals demonstrated a significant increase in the number of degenerating axons, both hyperdense and those with an accumulation of abnormal cytoskeletal organelles compared to WT tissue (16 949 ± 979/mm^2 vs. 169 ± 169/mm^2, Figure 3a, one-way ANOVA, $p < .001$). Restoration of neuronal *a-series* ganglioside expression in *Rescue* mice led to a significant reduction in degenerating axons (6,215 ± 1494/mm^2). While significantly lower than *Dbl KO* mice, the number remained greater than WT, suggesting a partial rescue of this feature and the potential need for *b-series* gangliosides for full rescue as shown in *GalNAcT*$^{-/-}$-*Tg(neuronal)* mice (Yao et al., 2014). Splitting of the myelin sheath was a feature of both *Dbl ko* and *Rescue* animals (indicated by arrowheads Figure 3a). To determine if the loss in CNS degenerating axon number corresponded to a loss in the number of NoR, we quantified Nav clusters flanked by Caspr dimers (representative images of immunostaining shown in Figure 4c). In the optic nerve, Nav cluster number was reduced in *Dbl KO* mice compared to WT (53.4 ± 0.77 vs. 72.4 ± 5.58, Figure 3a, one-way ANOVA, $p = .07$) and restored to WT levels in the *Rescue* mice (75.9 ± 8.44 vs. 72.4 ± 5.58, Figure 3a, one-way ANOVA, $p = .07$). These results do not reach significance but indicate a subtle reduction in nodes in response to complex ganglioside loss. Previous studies have shown that mice with limited ganglioside expression have a reduced number of motor neurons and increased F4/80 immunoreactivity and complement deposits in their lumbar spinal cord and cerebellum with age (Ohmi et al.,. ,2009, 2014). We set out to replicate these findings and determine if this could be reversed with the reintroduction of neuronal *a-series* ganglioside expression. Immunostaining for the neuronal marker NeuN showed a reduction in the number of positive motor neurones in the ventral horn of the cervical cord in *Dbl KO* mice compared to WT (17 ± 2 vs. 28 ± 1 cells/ROI, one-way ANOVA $p < .05$, Figure 3b). The number of NeuN-positive neurons increased when *a-series* gangliosides were reintroduced (23 ± 3 cells/ROI) but this did not reach significance compared to *Dbl KO* cord and simultaneously was not significantly reduced compared to WT, suggesting a partial rescue. The number of F4/80-positive cells, suggesting microglial activation, increased significantly in *Dbl KO* mice compared to WT (22 ± 4 vs. 10 ± 1 cells/ROI, one-way ANOVA $p < .05$, Figure 3b), and while *Rescue* mice had fewer positive cells (11 ± 3 cells/ROI), again this did not reach significance compared to either of the other genotypes. As had been previously reported by Ohmi et al. (2014), we observed an increase in immunoreactivity for complement (C3c) in *Dbl KO* spinal cord compared to WT. This immunoreactivity was qualitatively attenuated in the spinal cords from *Rescue* mice.

3.3 | Loss of CNS axo–glial integrity in Dbl KO mice is attenuated by neuronal a-series ganglioside expression

Complex ganglioside deficiency has been associated with age-dependent nodal disorganisation in myelinated fibres suggesting a role in stability and maintenance of this specialised site (Susuki, Baba, et al., 2007). This has not previously been investigated in *Dbl KO* mice, thus we characterised the nodal disorganisation of *Dbl KO* mice, and the role of neuronal *a-series* ganglioside expression in normalising this. In the CNS (optic nerve), the total length of pan-neurofascin (pNFasc) immunostaining (comprising both nodal NF186 and paranodal NF155

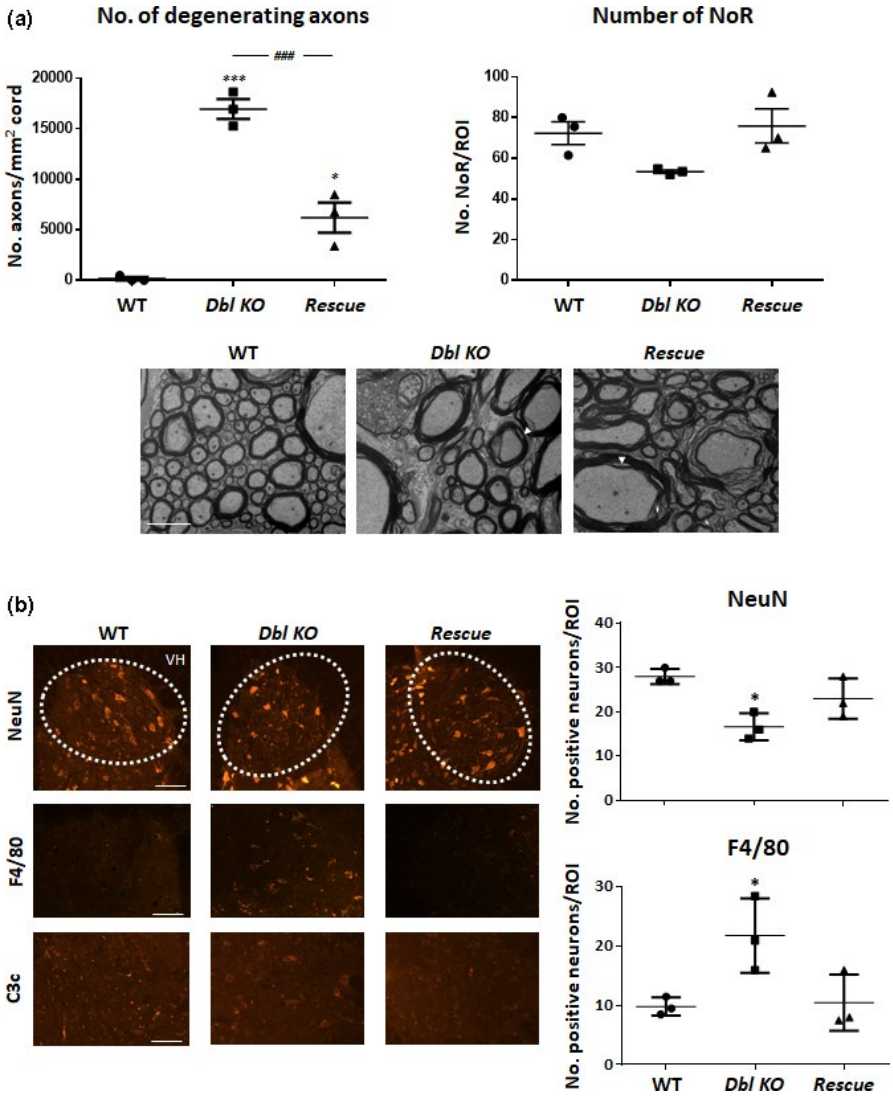

FIGURE 3 An increase in neurodegeneration and immune markers found in the CNS of 12-month-old *Dbl KO* mice is reversed by the expression of neuronal *a-series* gangliosides. (a) When *a-series* ganglioside expression is restored in *Rescue* cervical spinal cord, the number of degenerating axons significantly decreases compared to *Dbl KO* mice, but remains increased compared to WT, indicating a partial rescue of this feature. Representative micrographs are shown for each genotype; white arrowheads indicate myelin splitting. The number of mature nodes of Ranvier (NoR, voltage-gated sodium channel [Nav] clusters flanked by Caspr dimers, see Figure 4c for representative images) was reduced in 6-month CNS optic nerves of *Dbl KO* mice, however, this did not reach significance. This number was restored to WT levels by restoration of *a-series* gangliosides in neurons of *Rescue* mice. (b) The number of NeuN-positive neurons is reduced, and F4-80-positive cells is significantly increased in the cervical spinal cord ventral horn (VH) in *Dbl KO* mice compared to WT. Reconstitution of *a-series* ganglioside expression in *Rescue* mice partially restores these parameters to WT levels. C3c reactivity is observed in *Dbl KO* mice spinal cord. One-way ANOVA, * indicates significance compared to WT and # indicates significance compared to *Rescue*, $^{*}p < .05$, $^{***}p < .001$, $n = 3$ mice/genotype. Scale bar =5 μm (a) and 10 μm (b). Abbreviated nomenclature: Wild type (WT); $GD3s^{-/-} \times GalNAcT^{-/-}$ (*Dbl KO*); $GD3s^{-/-} \times GalNAc\text{-}T^{-/-}$-*Tg(neuronal)* (*Rescue*)

domains) was significantly reduced in *Dbl KO* mice compared to WT (2.4 ± 0.39 vs. 4.7 ± 0.23, Figure 4a, one-way ANOVA, $p < .01$). In all mice, the staining for NF186, defined by co-localisation with the nodal marker AnkyrinG, appeared strong and unaltered. Whilst paranodal NF155 staining was observed in *Dbl KO* mice (indicated by white arrowheads), many nodes consisted only of nodal NF186 staining (indicated by open arrowheads), thus accounting for the reduction in average pNFasc domain length. The length of pNFasc staining was recovered to within the range of WT length in *Rescue* mice and was significantly longer than *Dbl KO* mice (3.8 ± 0.04 vs. 2.4 ± 0.39, one-way ANOVA, $p < .05$). Similarly, total Caspr domain length was significantly reduced in *Dbl KO* mice compared to WT (2.9 ± 0.2 vs. 3.5 ± 0.05 μm, Figure 4c, one-way ANOVA, $p < .05$). The loss of staining most prominently occurred at the paranodal/juxtaparanodal border (open arrowheads, Figure 4c). However, unlike pNFasc, the length remained truncated in the *Rescue* compared to WT mice (2.8 ± 0.05 vs. 3.5 ± 0.05 μm, Figure 4c, one-way ANOVA, $p < .05$). Nav clusters occasionally appear lengthened in *Dbl KO* mice (white arrowheads).

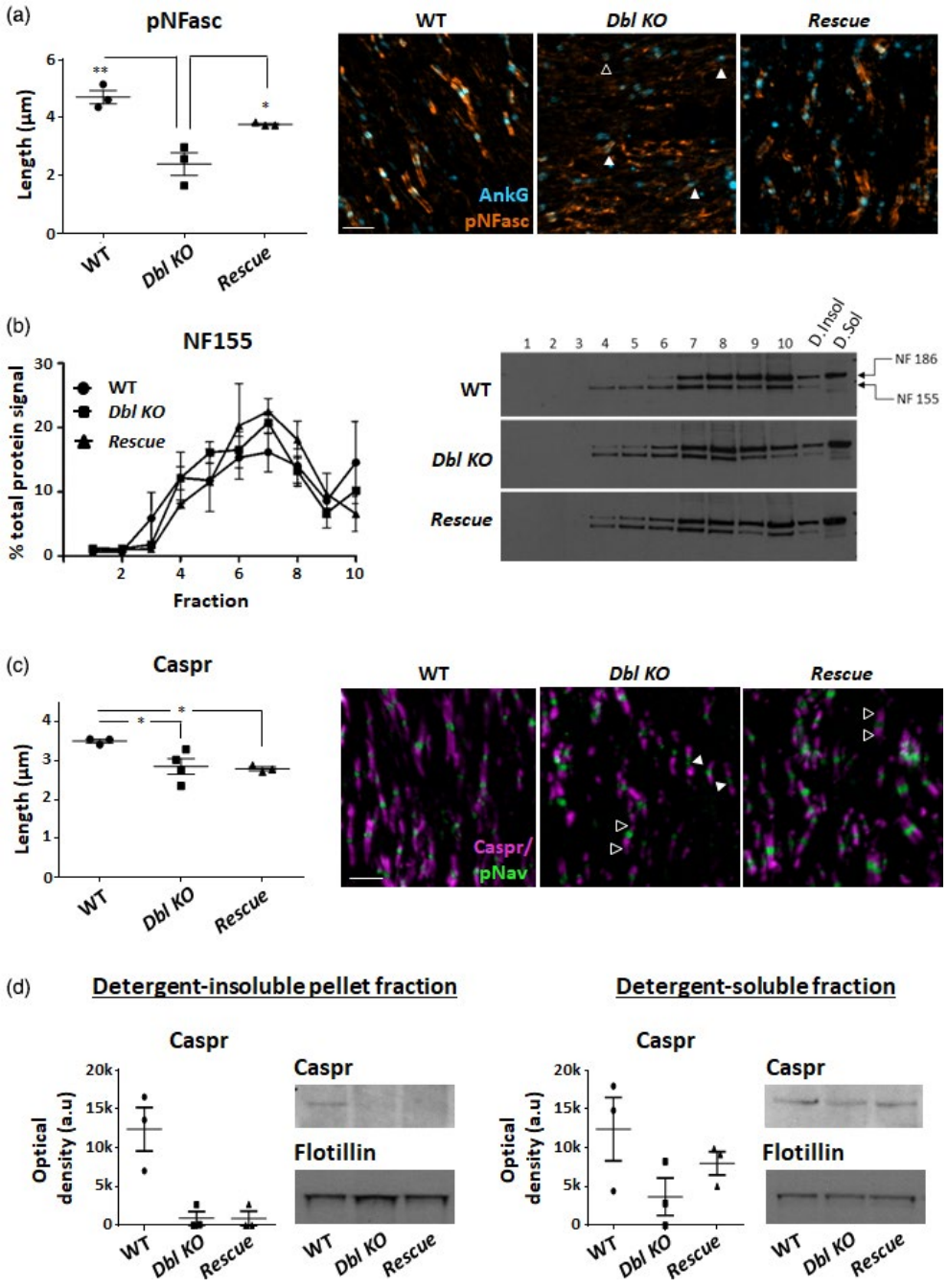

FIGURE 4 Age-dependent disturbance of CNS axo–glial integrity in *Dbl KO* mice is partially restored by neuronal *a-series* ganglioside expression. (a) Mature nodes of Ranvier (NoR) are identified by AnkyrinG clusters (blue) flanked by pan-neurofascin (pNFasc) dimers (orange). Total length of pNFasc (detects both nodal NF186 and paranodal NF155 isoforms) immunostaining in 6-month-old optic nerves is significantly reduced in *Dbl KO* mice, and restored to WT levels with neuronal *a-series* ganglioside expression in *Rescue* mice. In *Dbl KO* mice, presumed NF155 can be identified (white arrowheads), but often only presumed NF186 is present (open arrowhead). (b) Sucrose density gradient analysis of the TX-100 detergent-insoluble (D. Insol) fraction of brain membrane homogenate revealed no change in the lipid raft association of NF155 in *Dbl KO or Rescue* mice compared to WT. (c) Mature NoR are identified by pan voltage-gated sodium channel (pNav) clusters (green) flanked by paranodal Caspr dimers (magenta) in optic nerve. Total length of Caspr immunostaining is reduced in 6-month-old optic nerves of both *Dbl KO* and *Rescue* mice. Open arrowheads indicate shortening of Caspr staining at the paranodal/juxtaparanodal edge, and white arrowheads indicate examples of lengthened pNav cluster staining. (d) In WT brain membrane homogenate, Caspr was present in the detergent-soluble and detergent-insoluble fractions following extraction in TX-100 detergent, whereas almost all Caspr from *Dbl KO* and *Rescue* mice was found in the detergent-soluble fraction. Blots show that raft-associated Flotillin protein was mostly resistant to TX-100 extraction and present in all genotypes. One-way or two-way ANOVA, $^{*}p < .05$, $^{**}p < .01$, $n = 3$–4 mice/genotype. Scale bars =5 µm (a) and 20 µm (b). Abbreviated nomenclature: Wild type (WT); *GD3s*$^{-/-}$ × *GalNAcT*$^{-/-}$ (*Dbl KO*); *GD3s*$^{-/-}$ × *GalNAc-T*$^{-/-}$*-Tg(neuronal)* (*Rescue*)

Caspr and NF155 are tethered to detergent-insoluble lipid rafts and thought to be required for maintenance of paranodal architecture. Previous reports have shown disruption of lipid raft microdomains in the absence of gangliosides leading to an interruption in axo–glial integrity at the paranodal junction (Susuki, Baba, et al., 2007). Lipid rafts are a heterogeneous mixture of the lipids that associate with various proteins to generate an ordered membrane structure that can resist solubilisation by detergents. In this study, we employ a detergent extraction procedure followed by centrifugation that separates the lipid raft containing detergent-insoluble pellet from the detergent -soluble supernatant. The detergent-insoluble pool will contain proteins associated with lipid rafts but also protein aggregates and complexes that can resist detergent solubilisation. The detergent-soluble fraction will be composed of proteins associated with small cellular micelles. The proteins associated with lipid rafts can be further purified from the detergent-insoluble fraction by sucrose density ultracentrifugation because of the lipid-mediated low-density, positive buoyancy of the rafts that causes floatation to the low-density sucrose fractions. To test if loss of all gangliosides but GM3 causes raft disruption, we investigated the distribution of selected proteins in the detergent-soluble fraction and the detergent-insoluble fractions. The raft integrity was confirmed by pre-treatment with saponin to disrupt the cholesterol association with rafts and prevent the resistance to detergent solubilisation and therefore the floatation of selected proteins (NF155 and MAG) during sucrose ultracentrifugation (Figure S1a). Two detergent systems were used based on previous studies that have characterised their raft properties: Triton X-100 for Caspr, NF155 and flotillin (Ohmi et al., 2011; Susuki, Baba, et al., 2007) and CHAPS for the myelin-associated proteins PLP and MAG (Taylor et al., 2002). For NF155, Flotillin and MAG, a significant proportion of the total pool was present in the detergent-insoluble lipid raft containing fraction in all three genotypes (Figures 4b,d & 5b). However, while Caspr was present in the detergent-insoluble fraction in WT, it was not detected in the *Dbl KO* and *Rescue* genotypes (Figure 4d). This was not due to a global loss of Caspr as the protein was detected in the non-raft-associated detergent-soluble fraction in all genotypes (Figure 4d).

A more sensitive analysis was then performed using a floatation assay sucrose density centrifugation to isolate the lipid raft pool as a result of their lipid association mediated buoyancy properties. The intensity of the target protein detected in 10 fractions, collected from low to high sucrose density, is expressed as a % relative to the total intensity across all fractions. The profile for NF155 for each genotype displayed a shoulder in fractions 4–5 with a peak in abundance in fraction 6 (Figure 4b). There was no detectable difference between the genotypes in the distribution of NF155. Higher density fractions 7 onwards had detectable NF155 and NF186 reactivity. As NF186 does not fulfil the criteria for raft association (Schafer et al., 2004), these fractions are not regarded as lipid rafts. The profile for MAG was similar among WT, *DblKO* and *Rescue* mice with a peak abundance in fraction 4 for all genotypes (Figure 5a). Interestingly, we observed that the amount of MAG present in the non-raft detergent-soluble fraction was lower in ganglioside *Dbl KO* and *Rescue* genotypes relative to WT (Figure 5b). To gain greater

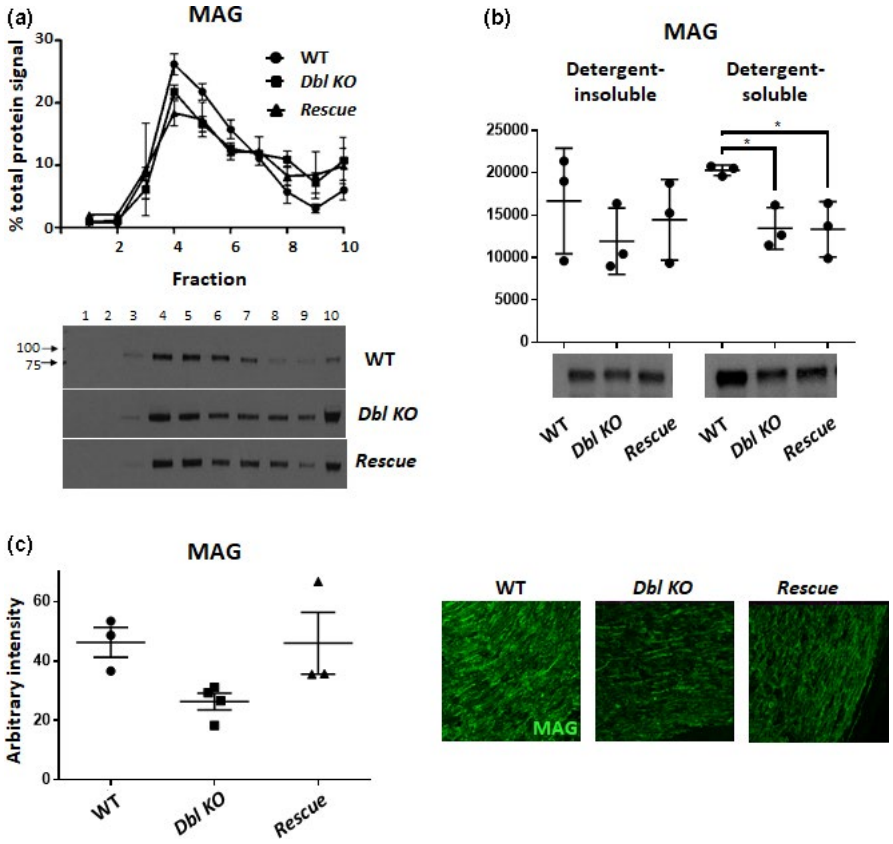

FIGURE 5 Lipid raft-associated myelin-associated glycoprotein (MAG) is not perturbed in *Dbl KO* mice but total brain levels are reduced. (a) Sucrose density gradient analysis of the CHAPS detergent-insoluble fraction of brain membrane homogenate revealed no change in the lipid raft association of MAG in *Dbl KO* or *Rescue* mice compared to WT. (b) MAG levels do not change in the detergent-insoluble fraction from brains among genotypes, but are reduced in the detergent-soluble fraction from both *Dbl KO* and *Rescue* mice. (c) A decrease in MAG (green) intensity is observed in optic nerve sections from *Dbl KO* mice and returns to WT levels with neuronal expression of *a-series* gangliosides in *Rescue* mice. One-way or two-way ANOVA, $*p < .05$, $n = 3–4$ mice/genotype. Scale bar =10 μm. Abbreviated nomenclature: Wild type (WT); *GD3s*$^{-/-}$ × *GalNAcT*$^{-/-}$ (*Dbl KO*); *GD3s*$^{-/-}$ × *GalNAc-T*$^{-/-}$*-Tg(neuronal)* (*Rescue*)

insight into the effect of complex ganglioside loss on the ganglioside ligand MAG, we assessed axo–glial MAG distribution by staining intensity in optic nerve sections. MAG intensity showed a reduction in *Dbl KO* mice compared to WT that was partially resolved in *Rescue* mice (26.4 ± 2.8 vs. 46.3 ± 5 vs. 46 ± 10.4 AU, Figure 5c, one-way ANOVA, $p < .05$, no significance in post-hoc multivariate comparisons). We also analysed PLP, a major compact myelin protein in one preparation and found that the raft profile was comparable for all three genotypes (Figure S1b).

Flotillin, which is regarded as a marker for lipid rafts, did display a rightward shift in the *Dbl KO* mice with a significantly lower proportion in fraction 4 when directly compared to WT (Figure S1c). However, when all three genotypes were compared, there was no difference among the flotillin profiles as Rescue displays intermediate properties. A high proportion of Caspr was detected in the raft-associated fractions from WT mice; however, only a very weak unmeasurable signal was detected in the *Dbl KO* and *Rescue* genotypes (Figure S1d). Taken together, the data suggest that there may be a discrete disruption of selected rafts present in distinct cellular membranes; there is a disruption to raft association in axonal proteins, but no major disruption of the rafts associated with the glial paranodal junction.

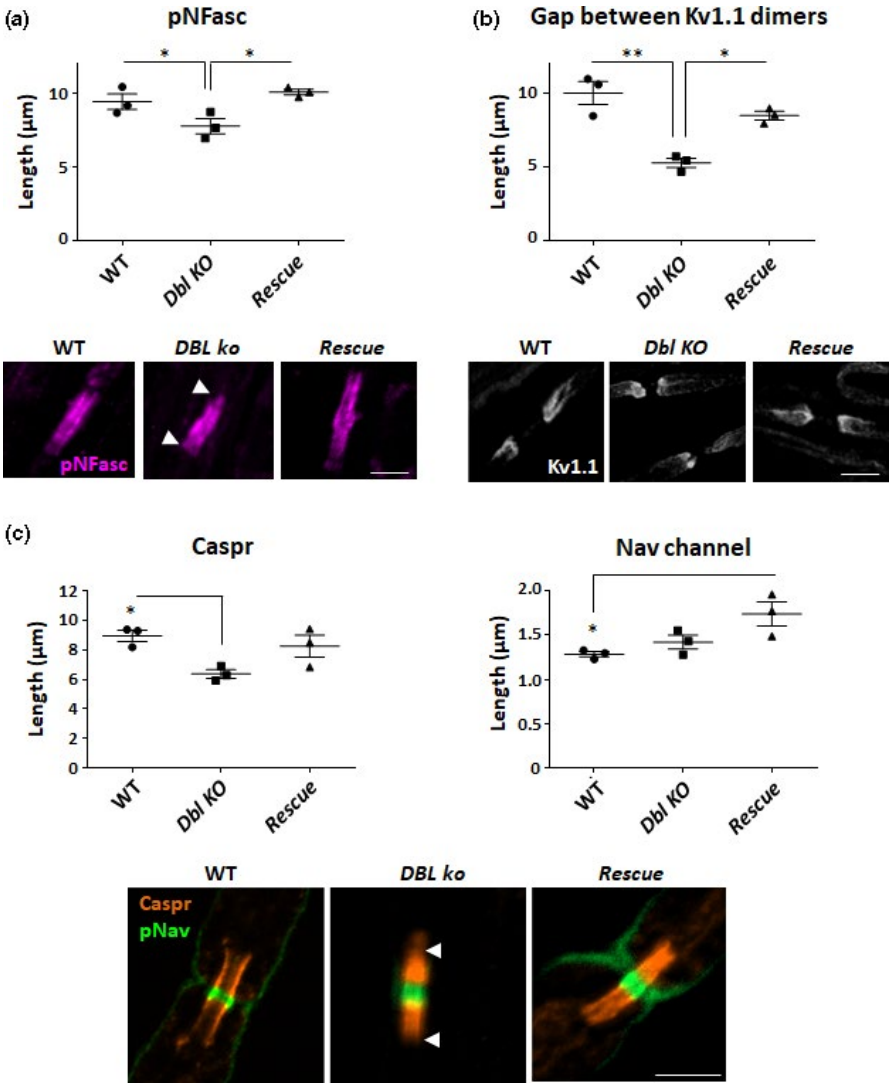

FIGURE 6 Age-dependent disturbance of PNS axo–glial integrity in *Dbl KO* mice is partially restored by neuronal expression of *a-series* gangliosides. (a) Total pan-neurofascin (pNFasc) immunostaining length (magenta, detects nodal NF186 and paranodal NF155) decreased in 6-month-old *Dbl KO* sciatic nerve nodes of Ranvier (NoR) and recovered with neuronal *a-series* ganglioside expression in *Rescue* nerve. Loss of staining was observed at the paranodal/juxtaparanodal edge (arrowheads). (b) A decrease in the length of gap between voltage-gated potassium channel (Kv1.1) dimers (white), indicating paranodal invasion, is observed in sciatic nerve from *Dbl KO* mice and returns to WT levels with neuronal expression of *a-series* gangliosides in *Rescue* mice. (c) A reduction in total Caspr staining length (orange) and lengthened pan voltage-gated sodium channel (pNav) clusters (green) was observed at sciatic nerve NoR from 6-month-old *Dbl KO* mice. Weaker Caspr staining at the juxtaparanodal edge of the paranode is indicated by arrowheads. Total Caspr length was normalised in *Rescue* mice and Nav cluster length further increased with restoration of neuronal *a-series* gangliosides. One-way ANOVA, $^{*}p < .05$, $^{**}p < .01$$^{***}p < .001$, $n = 3$ mice/genotype. Scale bars = 5 µm (A&B) and 10 µm (c). Abbreviated nomenclature: Wild type (WT); *GD3s*$^{-/-}$ × *GalNAcT*$^{-/-}$ (*Dbl KO*); *GD3s*$^{-/-}$ × *GalNAc-T*$^{-/-}$*-Tg(neuronal)* (*Rescue*)

3.4 | Disruption of PNS axo–glial integrity in Dbl KO mice is reversed by neuronal a-series ganglioside expression

In the PNS, GM3-only expression in *Dbl KO* mice resulted in a reduction in total pNFasc length, particularly at the paranodal/juxtaparanodal border compared to WT (7.8 ± 0.5 vs. 9.4 ± 0.5 μm, Figure 6a, one-way ANOVA, $p < .05$). Neuronal *a-series* ganglioside expression reversed the reduction in length to within the WT range in *Rescue* mice and was significantly lengthened compared to *Dbl KO* (10.1 ± 0.2 vs. 7.8 ± 0.5 μm, Figure 6a, one-way ANOVA, $p < .05$). This paranodal axo–glial disturbance was reflected by the reduction in distance between juxtaparanodal Kv1.1 dimer domains, suggestive of paranodal invasion owing to an impaired axo–glial junction. The gap between Kv1.1 dimers became significantly reduced in *Dbl KO* mice, and was restored within the range of WT values in *Rescue* nerve (5.3 ± 0.3 vs. 10.05 vs. 0.8 vs. 8.5 ± 0.3 μm, Figure 6b, one-way ANOVA, $p < .01$). Caspr length significantly decreased in *Dbl KO* mice compared to WT, and, unlike CNS tissue, this length was partially restored with *a-series* ganglioside expression (6.4 ± 0.3 vs. 8.97 ± 0.4 vs. 8.2 ± 0.8 μm, Figure 6c, one-way ANOVA, $p < .05$). A lengthening of Nav clusters in *Dbl KO* mice compared to WT was observed. This did not reach significance, however, the length was significantly greater in *Rescue* mice compared to WT and *Dbl KO* mice (1.29 ± 0.03 vs. 1.42 ± 0.08 vs. 1.74 ± 0.14, Figure 6c, one-way ANOVA, $p < .05$), a phenomenon we also observed in the *GalNAcT*$^{-/-}$*-Tg(neuronal)* mice (Yao et al., 2014). Reduction in length of Caspr immunostaining, because of a loss at the juxtaparanodal border of the paranode, is indicated by arrowheads.

4 | DISCUSSION

The role of individual gangliosides in neurodegeneration has been interrogated by transgenic manipulations at different stages in the biosynthesis pathway (Yu et al., 2011), but less is known about the contribution of more precise cellular membrane expression on phenotypes. GM1 & GD1a (*a-series*) and GD1b & GT1b (*b-series*) normally comprise the majority of nervous system gangliosides. We have previously shown that neuronal expression of these complex gangliosides is critical (Yao et al., 2014). Here, on the *Dbl KO* background, we reintroduced neuronal expression of the GalNAc-T gene to characterise the importance of *a-series* ganglioside expression selectively on neuronal membranes. Using behavioural, ultrastructural, immunohistological and biochemical methods, we compared the nervous system integrity of *Dbl KO*, *Rescue* and WT mice.

We show that neuronal *a-series* ganglioside expression is both necessary and sufficient for survival and normal behaviour. The essential role for gangliosides in sustaining life is indicated by early death in complete ganglioside-deficient mice (Yamamoto et al., 1996; Yoshihara et al., 2018), as is also seen in humans (Boukhris et al., 2013; Simpson et al., 2004). Survival in mice improves in *Dbl* KO mice, that express the simple ganglioside GM3, compared with complete ganglioside deficiency, but still does not result in a normal lifespan as we here, and others have shown (Inoue et al., 2002; Kawai et al., 2001). Early death has been attributed to lethal seizures and a neurodegenerative pathology incompatible with life. Selective reintroduction of complex gangliosides in neurons, but not glia, can attenuate age-dependent neurodegeneration found in *GalNAc-T*$^{-/-}$ mice (Yao et al., 2014), but it remains unknown if both *a-* and *b-series* gangliosides are essential. Considering *GD3s*$^{-/-}$ mice that solely express *a-series* gangliosides appear pathophysiologically normal (Okada et al., 2002), we surmised that *a-series* gangliosides are critical. In terms of survival, our results confirm that *a-series* ganglioside expression is sufficient; however, it is not possible to generate an exclusively *b-series* expressing mouse strain to ascertain their independent role.

In the *Dbl* KO strain, we have performed a detailed analysis of neurodegeneration and axo–glial integrity, and assessed the role of neuronally expressed *a-series* gangliosides in relation to these features. It was first reported that the absence of complex gangliosides led only to subtle nervous system defects (Takamiya et al., 1996), but the role of gangliosides in fine-tuning the nervous system is becoming better appreciated. The important role for complex gangliosides in maintaining nervous system integrity was first reported in an ensuing study by Sheikh, Sun, et al., (1999) who demonstrated myelin defects and axon degeneration in *GalNAc-T*$^{-/-}$ mice. In *Dbl KO* mice, peripheral nerve degeneration has been indicated, but not formally quantified (Inoue et al., 2002). Loss of neurons and up-regulation of inflammatory markers were previously reported in *Dbl KO* mice and provide a useful point of comparison in the current study (Ohmi et al.,. ,2009, 2014). Here, we performed an analysis of cervical spinal cord degenerating axons and found that there was a significant increase in the number of degenerating fibres compared to WT, which was partially rescued by neuronal *a-series* ganglioside expression. Myelin remained qualitatively abnormal in the presence of neuronal *a-series* gangliosides, which we interpret as a need for complex ganglioside expression in myelin or for a *b-series*-associated axonal ligand. Lipid raft association of myelin protein PLP remained normal suggesting this did not contribute to the observed myelin sheath splitting. In our *Dbl KO* mice, we reproduced the results reporting a reduction in spinal cord motor neuron number and show that once again the *Rescue* strain follows a similar pattern of partial recovery. This correlates with the increased number of degenerating axons, reduction in NoR and poor performance in behavioural tests assessing motor function. To uncover a mechanism for neurodegeneration, Ohmi et al. (2009) studied inflammatory and complement components in the brain of *Dbl KO* mice. Ganglioside deficiency in *Dbl KO* mice leads to the up-regulation of complement components in the brain, which the authors attributed to the dispersion of the complement regulators DAF and CD59 from lipid rafts. This was followed by consequent dysregulation of inflammatory mediators presumed to contribute to neurodegeneration. We too observed an increase in immunostaining for the inflammatory markers F4-80 and C3c in the

spinal cords from *Dbl KO* mice that was reversed by neuronal *a-series* ganglioside expression, lending support to the original observation; however, a more in-depth analysis would be required to fully understand the mechanism. Together these data show that neuronal *a-series* gangliosides can compensate for deficiencies and protect the nervous system to a sufficient degree that function is possible despite an incomplete return to WT levels, and that *b-series* gangliosides are required for complete normality.

NoR are essential for efficient nerve conduction and survival, and ganglioside expression is closely linked to this site (De Angelis et al., 2001; McGonigal et al., 2010; Sheikh, Deerinck, et al., 1999; Susuki, Baba, et al., 2007). Susuki, Baba, et al., (2007) were the first to demonstrate that aged *GalNAc-T*$^{-/-}$ mice display a disruption to the axo–glial junction at the paranode, and subsequent impairment in nerve function. There was a significant invasion of juxtaparanodal Kv domains into the PNS and CNS paranodes, and an additional shortening of the Caspr and NF155 paranodal protein domains in the CNS, demonstrating a breakdown of the axo–glial junction. This was similar though less pronounced, to the disruption observed in paranodal protein, sulfatide or GalC-deficient mice (Bhat et al., 2001; Boyle et al., 2001; Dupree et al., 1999; Ishibashi et al., 2002; Marcus et al., 2006; Tait et al., 2000). These results pointed towards a crucial role for complex gangliosides in maintenance of axo–glial integrity. Specifically, the authors suggested a critical role for *a-series* gangliosides as *GD3s*$^{-/-}$ mice show significantly less disruption. Previously, we replicated these results in *GalNAc-T*$^{-/-}$ mice, and additionally demonstrated that selectively expressing both *a-* and *b-series* complex gangliosides on neuronal, but not glial, membranes was enough to largely reverse this nodal pathology (Yao et al., 2014). Nodal disruption has not previously been investigated in *Dbl KO* mice, but the expectation was that nodal pathology would be similar or more severe than *GalNAc-T*$^{-/-}$ mice in the additional absence of GD3 since complete ganglioside-deficient mice have no transverse bands at the paranodal axo–glial junction (Yamashita et al., 2005). We found that both in the CNS and PNS, there was a loss or dispersion of Caspr and NF155 immunostaining at the juxtaparanodal edge of the paranode suggesting a breakdown in lateral paranodal axo–glial integrity, which was slightly more severe in the PNS than observed for *GalNAc-T*$^{-/-}$ mice. In the PNS, we observed an invasion of juxtaparanodal Kv1.1 channel clusters into the paranode and a lengthening of the Nav domain. Taken together, these data suggest that GM3 is not sufficient to maintain axo–glial integrity, particularly at the lateral paranode in *Dbl KO* mice.

Normal NF155 immunolocalisation was restored by neuronal *a-series* ganglioside expression in the CNS and PNS of *Rescue* mice; however, Caspr immunostaining was not improved in the CNS and only partially in the PNS. To independently validate our immunostaining data, we performed lipid raft analysis. Caspr and NF155 are interacting proteins (Charles et al., 2002) known to be stabilised in paranodal lipid rafts (Ogawa & Rasband, 2009) and their association with lipid raft fractions is impaired by complex ganglioside deficiency (Susuki, Baba, et al., 2007). Therefore, we studied whether lipid raft instability was exacerbated in *Dbl KO* mice and the role of neuronally expressed *a-series* gangliosides in recovering this. In this study, we show that lipid rafts are disrupted by ganglioside deficiency in *Dbl KO* mice based on a shift of the lipid raft marker flotillin out of the low-density raft-associated fractions, as previously shown (Ohmi et al., 2009). CNS NF155 lipid raft association did not appear perturbed in *Dbl KO* or *Rescue* brains. It is noteworthy that previously only ~20% of NF155 from the pure white matter optic nerve tract, displayed characteristics of lipid raft association (Schafer et al., 2004) and a reduction in the proportion of protein that is raft associated, rather than a complete loss of raft association, based on a sucrose gradient taken from whole brains of *GalNAc-T*$^{-/-}$ compared to WT is observed (Susuki, Baba, et al., 2007). In addition, from our immunostaining data, the domain that is disrupted at the juxtaparanodal/paranodal edge is very minor in size relative to the whole brain. Taken together, it is possible that any changes in NF155 raft association were not detectable in this study because of an issue of sensitivity. Another interpretation for the discrepancy could be that NF155 associates with sulfatide rather than ganglioside-enriched rafts (Palavicini et al., 2016; Schafer et al., 2004). Therefore, a proportion of NF155 remains associated with rafts but its localisation, as determined by immunostaining, is dispersed due to mislocalisation of the axo–glial binding partner Caspr. This could be recovered in *a-series* neuronal rescue despite undetectable Caspr levels due to a differential stability of protein partners. Previous reports have shown that after initial formation, a post-developmental induction of glial NF155 knock-down causes a temporal delay in loss of Caspr (Pillai et al., 2009), so the reverse is also possible.

In contrast to NF155, we showed that the raft association of Caspr was impaired in the *Dbl KO* and was not improved by neuronal *a-series* expression in *Rescue* mice, which aligns with our immunostaining results. It is somewhat surprising that *a-series* neuronal ganglioside expression did not improve axonal Caspr staining or raft association, and suggests that Caspr requires stabilisation by *b-series* ganglioside-enriched rafts, at least at the juxtaparanodal/paranodal edge. Caspr (and possibly NF155) is likely also restricted to the paranode by the axo–glial junction formed by MAG interaction with neuronal ganglioside (Pronker et al., 2016) at the juxtaparanodal border. Thus, Caspr might be stabilised by two mechanisms and it is the sum of these protein–protein and protein–lipid interactions that lead to stability of the axo–glial junction.

MAG, found on the adaxonal myelin membrane apposing the axon, is a key ligand for gangliosides and a vital component for stability along the length of the axo–glial junction (Bartsch et al., 1989; Schnaar et al., 1998; Trapp et al., 1989). Similarities in *GalNAc-T*$^{-/-}$ and MAG$^{-/-}$ age-dependent neurodegenerative phenotypes and the significant reduction in MAG protein in the CNS of *GalNAc-T*$^{-/-}$ mice have been noted (McGonigal et al., 2019; Sheikh, Sun, et al., 1999) and signify the importance of this axo–glial partnership. The main ligands for MAG are GT1b and GD1a (Collins et al., 1997; Vinson et al., 2001). In the CNS, we showed a reduction in MAG intensity in *Dbl KO* mice, which was partially recovered in *Rescue* mice. The total amount of MAG in the detergent-soluble fraction (non-raft) decreased in both

Dbl KO and *Rescue* mice compared to WT and likely accounts for the loss in immunostaining, but lipid raft association was not perturbed in any genotype. Extraction studies suggest that MAG is anchored by sulfatide containing lipid rafts (Pomicter et al., 2013) which are likely unaltered in *Dbl KO* mice as sulfatide levels do not change in the absence of gangliosides, and vice versa (Honke et al., 2002; Yamashita et al., 2005). It would seem the axo–glial interaction between glial MAG and neuronal GT1b and GD1a has been disturbed in the *Dbl KO* mice, accounting for reduced staining intensity along the nerve, and GD1a ganglioside alone was insufficient to completely recover this interaction and MAG localisation in *Rescue* mice. We recently reported that sulfatide and gangliosides play independent roles in axo–glial stability and it is their combined deficiency that is lethal (McGonigal et al., 2019). We proposed a critical role for ganglioside/MAG interaction in the absence of sulfatide that was exacerbated in the absence of *b-series* gangliosides (McGonigal et al., 2019). In the current scenario, it seems that the influence of *a-series* gangliosides is also insufficient to suppress the axo–glial disorganisation. Transgenic mice lacking key sialylation enzymes resulting in severely diminished expression of GD1a and GT1b, had significantly lower brain MAG expression (Sturgill et al., 2012). This transgenic mouse shows the significance of GT1b to MAG localisation and a normal nervous system. Together these data further emphasise the importance of *b-series* gangliosides in axo–glial integrity.

As discussed in our original characterisation of *GalNAc-T*$^{-/-}$*-Tg(neuronal)* rescue mice, the activity of normal GalNAc-T enzyme in whole brain is not completely restored (Yao et al., 2014), as would be expected when adopting an approach using an unrelated promoter to drive expression that is normally highly restricted spatially and temporally. As such, it is possible that incomplete restoration of *Rescue* mice to normal might partially be explained by suboptimal enzyme activity. Total ganglioside content remains unchanged by genetic alteration due to over-expression of simple gangliosides, which could incompletely compensate and only partially restore function. Gangliosides are a large and dynamic family of lipids involved in diverse functions from cell–cell recognition to neural development. There is considerable membrane and subcellular heterogeneity in ganglioside expression throughout the body, and additionally there is likely a high degree of heterogeneity in lipid raft composition—one study, for example, demonstrates distinct separation between GM1- and GD3-containing rafts (Vyas et al., 2001). These factors can all uniquely influence and contribute to the phenotype and neurodegeneration found in *Dbl KO* mice. We could not exhaustively study every aspect of ganglioside function, so here report on key sites of interest in myelinated nerve organisation and maintenance. Overall, our findings build upon and enhance our understanding of the role of gangliosides in nervous system integrity, with a particular focus on the node of Ranvier.

ACKNOWLEDGEMENTS

This work was supported by the Wellcome Trust (grant numbers 092805, 202789), and LB was supported by University of Glasgow Vet Fund.

All experiments were conducted in compliance with the ARRIVE guidelines.

CONFLICT OF INTEREST

The authors have no conflicts of interest to declare.

DATA AVAILABILITY STATEMENT

Data available on request from the authors.

ORCID

Rhona McGonigal https://orcid.org/0000-0001-9571-2526
Jennifer A. Barrie https://orcid.org/0000-0003-0378-6865
Lauren E. Black https://orcid.org/0000-0001-5459-7939
Mark McLaughlin https://orcid.org/0000-0001-5317-2090
Hugh J. Willison https://orcid.org/0000-0002-5997-1683

REFERENCES

Bartsch, U., Kirchhoff, F., & Schachner, M. (1989). Immunohistological localization of the adhesion molecules L1, N-CAM, and MAG in the developing and adult optic nerve of mice. *The Journal of Comparative Neurology*, *284*, 451–462. https://doi.org/10.1002/cne.902840310

Bhat, M. A., Rios, J. C., Lu, Y., Garcia-Fresco, G. P., Ching, W., Martin, M. S., Li, J., Einheber, S., Chesler, M., Rosenbluth, J., Salzer, J. L., & Bellen, H. J. (2001). Axon-glia interactions and the domain organization of myelinated axons requires neurexin IV/Caspr/Paranodin. *Neuron*, *30*, 369–383. https://doi.org/10.1016/S0896-6273(01)00294-X

Boffey, J., Odaka, M., Nicoll, D., Wagner, E. R., Townson, K., Bowes, T., Conner, J., Furukawa, K., & Willison, H. J. (2005). Characterisation of the immunoglobulin variable region gene usage encoding the murine anti-ganglioside antibody repertoire. *Journal of Neuroimmunology*, *165*, 92–103. https://doi.org/10.1016/j.jneuroim.2005.04.011

Boukhris, A., Schule, R., Loureiro, J. L., Lourenço, C. M., Mundwiller, E., Gonzalez, M. A., Charles, P., Gauthier, J., Rekik, I., Acosta Lebrigio, R. F., Gaussen, M., Speziani, F., Ferbert, A., Feki, I., Caballero-Oteyza, A., Dionne-Laporte, A., Amri, M., Noreau, A., Forlani, S., … Stevanin, G. (2013). Alteration of ganglioside biosynthesis responsible for complex hereditary spastic paraplegia. *American Journal of Human Genetics*, *93*, 118–123. https://doi.org/10.1016/j.ajhg.2013.05.006

Bowes, T., Wagner, E. R., Boffey, J. et al (2002). Tolerance to self gangliosides is the major factor restricting the antibody response to lipopolysaccharide core oligosaccharides in Campylobacter jejuni strains associated with Guillain-Barre syndrome. *Infection and Immunity*, *70*, 5008–5018.

Boyle, M. E., Berglund, E. O., Murai, K. K., Weber, L., Peles, E., & Ranscht, B. (2001). Contactin orchestrates assembly of the septate-like junctions at the paranode in myelinated peripheral nerve. *Neuron*, *30*, 385–397. https://doi.org/10.1016/S0896-6273(01)00296-3

Cerneus, D. P., Ueffing, E., Posthuma, G., Strous, G. J., & van der Ende, A. (1993). Detergent insolubility of alkaline phosphatase during biosynthetic transport and endocytosis. Role of cholesterol. *The Journal of Biological Chemistry*, *268*, 3150–3155. https://doi.org/10.1016/S0021-9258(18)53671-1

Charles, P., Tait, S., Faivre-Sarrailh, C., Barbin, G., Gunn-Moore, F., Denisenko-Nehrbass, N., Guennoc, A.-M., Girault, J.-A., Brophy, P. J., & Lubetzki, C. (2002). Neurofascin is a glial receptor for the paranodin/Caspr-contactin axonal complex at the axoglial junction. *Current Biology*, *12*, 217–220. https://doi.org/10.1016/S0960-9822(01)00680-7

Collins, B. E., Yang, L. J., Mukhopadhyay, G., Filbin, M. T., Kiso, M., Hasegawa, A., & Schnaar, R. L. (1997). Sialic acid specificity of

myelin-associated glycoprotein binding. *The Journal of Biological Chemistry*, *272*, 1248–1255. https://doi.org/10.1074/jbc.272.2.1248

De Angelis, M. V., Di Muzio, A., Lupo, S., Gambi, D., Uncini, A., & Lugaresi, A. (2001). Anti-GD1a antibodies from an acute motor axonal neuropathy patient selectively bind to motor nerve fiber nodes of Ranvier. *Journal of Neuroimmunology*, *121*, 79–82. https://doi.org/10.1016/S0165-5728(01)00434-9

Dupree, J. L., Girault, J. A., & Popko, B. (1999). Axo-glial interactions regulate the localization of axonal paranodal proteins. *The Journal of Cell Biology*, *147*, 1145–1152. https://doi.org/10.1083/jcb.147.6.1145

Griffin, J. W., Li, C. Y., Macko, C., Ho, T. W., Hsieh, S.-T., Xue, P., Wang, F. A., Cornblath, D. R., McKhann, G. M., & Asbury, A. K. (1996). Early nodal changes in the acute motor axonal neuropathy pattern of the Guillain-Barré syndrome. *Journal of Neurocytology*, *25*, 33–51. https://doi.org/10.1007/BF02284784

Griffiths, I. R., Duncan, I. D., & McCulloch, M. (1981). Shaking pups: A disorder of central myelination in the spaniel dog. II. Ultrastructural observations on the white matter of the cervical spinal cord. *Journal of Neurocytology*, *10*, 847–858. https://doi.org/10.1007/BF01262657

Honke, K., Hirahara, Y., Dupree, J., Suzuki, K., Popko, B., Fukushima, K., Fukushima, J., Nagasawa, T., Yoshida, N., Wada, Y., & Taniguchi, N. (2002). Paranodal junction formation and spermatogenesis require sulfoglycolipids. *Proceedings of the National Academy of Sciences of the United States of America*, *99*, 4227–4232. https://doi.org/10.1073/pnas.032068299

Inoue, M., Fujii, Y., Furukawa, K., Okada, M., Okumura, K., Hayakawa, T., Furukawa, K., & Sugiura, Y. (2002). Refractory skin injury in complex knock-out mice expressing only the GM3 ganglioside. *The Journal of Biological Chemistry*, *277*, 29881–29888. https://doi.org/10.1074/jbc.M201631200

Ishibashi, T., Dupree, J. L., Ikenaka, K., Hirahara, Y., Honke, K., Peles, E., Popko, B., Suzuki, K., Nishino, H., & Baba, H. (2002). A myelin galactolipid, sulfatide, is essential for maintenance of ion channels on myelinated axon but not essential for initial cluster formation. *The Journal of Neuroscience: The Official Journal of the Society for Neuroscience*, *22*, 6507–6514. https://doi.org/10.1523/JNEUROSCI.22-15-06507.2002

Kawai, H., Allende, M. L., Wada, R., Kono, M., Sango, K., Deng, C., Miyakawa, T., Crawley, J. N., Werth, N., Bierfreund, U., Sandhoff, K., & Proia, R. L. (2001). Mice expressing only monosialoganglioside GM3 exhibit lethal audiogenic seizures. *The Journal of Biological Chemistry*, *276*, 6885–6888. https://doi.org/10.1074/jbc.C000847200

Marcus, J., Dupree, J. L., & Popko, B. (2002). Myelin-associated glycoprotein and myelin galactolipids stabilize developing axo-glial interactions. *The Journal of Cell Biology*, *156*, 567–577. https://doi.org/10.1083/jcb.200111047

Marcus, J., Honigbaum, S., Shroff, S., Honke, K., Rosenbluth, J., & Dupree, J. L. (2006). Sulfatide is essential for the maintenance of CNS myelin and axon structure. *Glia*, *53*, 372–381. https://doi.org/10.1002/glia.20292

McGonigal, R., Cunningham, M. E., Yao, D., Barrie, J. A., Sankaranarayanan, S., Fewou, S. N., Furukawa, K., Yednock, T. A., & Willison, H. J. (2016). C1q-targeted inhibition of the classical complement pathway prevents injury in a novel mouse model of acute motor axonal neuropathy. *Acta neuropathologica communications*, *4*, 23. https://doi.org/10.1186/s40478-016-0291-x.

McGonigal R, Barrie J. A., Yao D., McLaughlin M., Cunningham M. E., Rowan E. G., Willison H. J. (2019). Glial sulfatides and neuronal complex gangliosides are functionally interdependent in maintaining myelinating axon integrity. *The Journal of Neuroscience*, *39*, (1), 63–77. http://doi.org/10.1523/jneurosci.2095-18.2018.

McGonigal, R., Rowan, E. G., Greenshields, K. N., Halstead, S. K., Humphreys, P. D., Rother, R. P., Furukawa, K., & Willison, H. J. (2010). Anti-GD1a antibodies activate complement and calpain to injure distal motor nodes of Ranvier in mice. *Brain*, *133*, 1944–1960. https://doi.org/10.1093/brain/awq119

Merritt, E. A., Sarfaty, S., van den Akker, F., L'Hoir, C., Martial, J. A., & Hol, W. G. (1994). Crystal structure of cholera toxin B-pentamer bound to receptor GM1 pentasaccharide. *Protein Science*, *3*, 166–175.

Ogawa, Y., & Rasband, M. N. (2009). Proteomic analysis of optic nerve lipid rafts reveals new paranodal proteins. *Journal of Neuroscience Research*, *87*, 3502–3510.

Ogawa-Goto, K., & Abe, T. (1998). Gangliosides and glycosphingolipids of peripheral nervous system myelins–a minireview. *Neurochemical Research*, *23*, 305–310.

Ohmi, Y., Ohkawa, Y., Tajima, O., Sugiura, Y., Furukawa, K., & Furukawa, K. (2014). Ganglioside deficiency causes inflammation and neurodegeneration via the activation of complement system in the spinal cord. *Journal of Neuroinflammation*, *11*, 61. https://doi.org/10.1186/1742-2094-11-61

Ohmi, Y., Tajima, O., Ohkawa, Y., Mori, A., Sugiura, Y., Furukawa, K., & Furukawa, K. (2009). Gangliosides play pivotal roles in the regulation of complement systems and in the maintenance of integrity in nerve tissues. *Proceedings of the National Academy of Sciences of the United States of America*, *106*, 22405–22410. https://doi.org/10.1073/pnas.0912336106

Ohmi, Y., Tajima, O., Ohkawa, Y., Yamauchi, Y., Sugiura, Y., Furukawa, K., & Furukawa, K. (2011). Gangliosides are essential in the protection of inflammation and neurodegeneration via maintenance of lipid rafts: Elucidation by a series of ganglioside-deficient mutant mice. *Journal of Neurochemistry*, *116*, 926–935. https://doi.org/10.1111/j.1471-4159.2010.07067.x

Okada, M., Itoh, M.-I., Haraguchi, M., Okajima, T., Inoue, M., Oishi, H., Matsuda, Y., Iwamoto, T., Kawano, T., Fukumoto, S., Miyazaki, H., Furukawa, K., Aizawa, S., & Furukawa, K. (2002). b-series Ganglioside deficiency exhibits no definite changes in the neurogenesis and the sensitivity to Fas-mediated apoptosis but impairs regeneration of the lesioned hypoglossal nerve. *The Journal of Biological Chemistry*, *277*, 1633–1636. https://doi.org/10.1074/jbc.C100395200

Palavicini, J. P., Wang, C., Chen, L., Ahmar, S., Higuera, J. D., Dupree, J. L., & Han, X. (2016). Novel molecular insights into the critical role of sulfatide in myelin maintenance/function. *Journal of Neurochemistry*, *139*, 40–54. https://doi.org/10.1111/jnc.13738

Pillai, A. M., Thaxton, C., Pribisko, A. L., Cheng, J. G., Dupree, J. L., & Bhat, M. A. (2009). Spatiotemporal ablation of myelinating glia-specific neurofascin (Nfasc NF155) in mice reveals gradual loss of paranodal axoglial junctions and concomitant disorganization of axonal domains. *Journal of Neuroscience Research*, *87*, 1773–1793.

Pomicter, A. D., Deloyht, J. M., Hackett, A. R., Purdie, N., Sato-Bigbee, C., Henderson, S. C., & Dupree, J. L. (2013). Nfasc155H and MAG are specifically susceptible to detergent extraction in the absence of the myelin sphingolipid sulfatide. *Neurochemical Research*, *38*, 2490–2502. https://doi.org/10.1007/s11064-013-1162-5

Pronker, M. F., Lemstra, S., Snijder, J., Heck, A. J., Thies-Weesie, D. M., Pasterkamp, R. J., & Janssen, B. J. (2016). Structural basis of myelin-associated glycoprotein adhesion and signalling. *Nature Communications*, *7*, 13584. https://doi.org/10.1038/ncomms13584

Rothberg, K. G., Ying, Y. S., Kamen, B. A., & Anderson, R. G. (1990). Cholesterol controls the clustering of the glycophospholipid-anchored membrane receptor for 5-methyltetrahydrofolate. *The Journal of Cell Biology*, *111*, 2931–2938. https://doi.org/10.1083/jcb.111.6.2931

Schafer, D. P., Bansal, R., Hedstrom, K. L., Pfeiffer, S. E., & Rasband, M. N. (2004). Does paranode formation and maintenance require partitioning of neurofascin 155 into lipid rafts? *The Journal of Neuroscience: The Official Journal of the Society for Neuroscience*, *24*, 3176–3185. https://doi.org/10.1523/JNEUROSCI.5427-03.2004

Schnaar, R. L., Collins, B. E., Wright, L. P., Kiso, M., Tropak, M. B., Roder, J. C., & Crocker, P. R. (1998). Myelin-associated glycoprotein binding to gangliosides. Structural specificity and functional implications.

Annals of the New York Academy of Sciences, *845*, 92–105. https://doi.org/10.1111/j.1749-6632.1998.tb09664.x

Schnaar, R. L., & Lopez, P. H. (2009). Myelin-associated glycoprotein and its axonal receptors. *Journal of Neuroscience Research*, *87*, 3267–3276.

Sheikh, K. A., Deerinck, T. J., Ellisman, M. H., & Griffin, J. W. (1999). The distribution of ganglioside-like moieties in peripheral nerves. *Brain*, *122*(Pt 3), 449–460. https://doi.org/10.1093/brain/122.3.449

Sheikh, K. A., Sun, J., Liu, Y., Kawai, H., Crawford, T. O., Proia, R. L., Griffin, J. W., & Schnaar, R. L. (1999). Mice lacking complex gangliosides develop Wallerian degeneration and myelination defects. *Proceedings of the National Academy of Sciences of the United States of America*, *96*, 7532–7537. https://doi.org/10.1073/pnas.96.13.7532

Simpson, M. A., Cross, H., Proukakis, C., Priestman, D. A., Neville, D. C. A., Reinkensmeier, G., Wang, H., Wiznitzer, M., Gurtz, K., Verganelaki, A., Pryde, A., Patton, M. A., Dwek, R. A., Butters, T. D., Platt, F. M., & Crosby, A. H. (2004). Infantile-onset symptomatic epilepsy syndrome caused by a homozygous loss-of-function mutation of GM3 synthase. *Nature Genetics*, *36*, 1225–1229. https://doi.org/10.1038/ng1460

Sturgill, E. R., Aoki, K., Lopez, P. H. H., Colacurcio, D., Vajn, K., Lorenzini, I., Majić, S., Yang, W. H., Heffer, M., Tiemeyer, M., Marth, J. D., & Schnaar, R. L. (2012). Biosynthesis of the major brain gangliosides GD1a and GT1b. *Glycobiology*, *22*, 1289–1301. https://doi.org/10.1093/glycob/cws103

Susuki, K., Baba, H., Tohyama, K., Kanai, K., Kuwabara, S., Hirata, K., Furukawa, K., Furukawa, K., Rasband, M. N., & Yuki, N. (2007). Gangliosides contribute to stability of paranodal junctions and ion channel clusters in myelinated nerve fibers. *Glia*, *55*, 746–757. https://doi.org/10.1002/glia.20503

Susuki, K., Rasband, M. N., Tohyama, K., Koibuchi, K., Okamoto, S., Funakoshi, K., Hirata, K., Baba, H., & Yuki, N. (2007). Anti-GM1 antibodies cause complement-mediated disruption of sodium channel clusters in peripheral motor nerve fibers. *The Journal of Neuroscience: The Official Journal of the Society for Neuroscience*, *27*, 3956–3967. https://doi.org/10.1523/JNEUROSCI.4401-06.2007

Svennerholm, L., Boström, K., Fredman, P., Jungbjer, B., Lekman, A., Månsson, J. E., & Rynmark, B. M. (1994). Gangliosides and allied glycosphingolipids in human peripheral nerve and spinal cord. *Biochimica Et Biophysica Acta*, *1214*, 115–123. https://doi.org/10.1016/0005-2760(94)90034-5

Tait, S., Gunn-Moore, F., Collinson, J. M., Huang, J., Lubetzki, C., Pedraza, L., Sherman, D. L., Colman, D. R., & Brophy, P. J. (2000). An oligodendrocyte cell adhesion molecule at the site of assembly of the paranodal axo-glial junction. *The Journal of Cell Biology*, *150*, 657–666. https://doi.org/10.1083/jcb.150.3.657

Takamiya, K., Yamamoto, A., Furukawa, K., Yamashiro, S., Shin, M., Okada, M., Fukumoto, S., Haraguchi, M., Takeda, N., Fujimura, K., Sakae, M., Kishikawa, M., Shiku, H., Furukawa, K., & Aizawa, S. (1996). Mice with disrupted GM2/GD2 synthase gene lack complex gangliosides but exhibit only subtle defects in their nervous system. *Proceedings of the National Academy of Sciences of the United States of America*, *93*, 10662–10667. https://doi.org/10.1073/pnas.93.20.10662

Taylor, C. M., Coetzee, T., & Pfeiffer, S. E. (2002). Detergent-insoluble glycosphingolipid/cholesterol microdomains of the myelin membrane. *Journal of Neurochemistry*, *81*, 993–1004. https://doi.org/10.1046/j.1471-4159.2002.00884.x

Trapp, B. D., Andrews, S. B., Wong, A., O'Connell, M., & Griffin, J. W. (1989). Co-localization of the myelin-associated glycoprotein and the microfilament components, F-actin and spectrin, in Schwann cells of myelinated nerve fibres. *Journal of Neurocytology*, *18*, 47–60. https://doi.org/10.1007/BF01188423

Vajn, K., Viljetić, B., Degmečić, I. V., Schnaar, R. L., & Heffer, M. (2013). Differential distribution of major brain gangliosides in the adult mouse central nervous system. *PLoS One*, *8*, e75720. https://doi.org/10.1371/journal.pone.0075720

Vinson, M., Strijbos, P. J., Rowles, A., Facci, L., Moore, S. E., Simmons, D. L., & Walsh, F. S. (2001). Myelin-associated glycoprotein interacts with ganglioside GT1b. A mechanism for neurite outgrowth inhibition. *The Journal of Biological Chemistry*, *276*, 20280–20285. https://doi.org/10.1074/jbc.M100345200

Vyas, K. A., Patel, H. V., Vyas, A. A., & Schnaar, R. L. (2001). Segregation of gangliosides GM1 and GD3 on cell membranes, isolated membrane rafts, and defined supported lipid monolayers. *Biological Chemistry*, *382*, 241–250. https://doi.org/10.1515/BC.2001.031

Willison, H. J., & Yuki, N. (2002). Peripheral neuropathies and anti-glycolipid antibodies. *Brain*, *125*, 2591–2625. https://doi.org/10.1093/brain/awf272

Yamamoto, A., Haraguchi, M., Yamashiro, S., Fukumoto, S., Furukawa, K., Takamiya, K., Atsuta, M., Shiku, H., & Furukawa, K. (1996). Heterogeneity in the expression pattern of two ganglioside synthase genes during mouse brain development. *Journal of Neurochemistry*, *66*, 26–34. https://doi.org/10.1046/j.1471-4159.1996.66010026.x

Yamashita, T., Wu, Y.-P., Sandhoff, R., Werth, N., Mizukami, H., Ellis, J. M., Dupree, J. L., Geyer, R., Sandhoff, K., & Proia, R. L. (2005). Interruption of ganglioside synthesis produces central nervous system degeneration and altered axon-glial interactions. *Proceedings of the National Academy of Sciences of the United States of America*, *102*, 2725–2730. https://doi.org/10.1073/pnas.0407785102

Yao, D., McGonigal, R., Barrie, J. A., Cappell, J., Cunningham, M. E., Meehan, G. R., Fewou, S. N., Edgar, J. M., Rowan, E., Ohmi, Y., Furukawa, K., Furukawa, K., Brophy, P. J., & Willison, H. J. (2014). Neuronal expression of GalNAc transferase is sufficient to prevent the age-related neurodegenerative phenotype of complex ganglioside-deficient mice. *The Journal of Neuroscience: The Official Journal of the Society for Neuroscience*, *34*, 880–891. https://doi.org/10.1523/JNEUROSCI.3996-13.2014

Yoshihara, T., Satake, H., Nishie, T., Okino, N., Hatta, T., Otani, H., Naruse, C., Suzuki, H., Sugihara, K., Kamimura, E., Tokuda, N., Furukawa, K., Fururkawa, K., Ito, M., & Asano, M. (2018). Lactosylceramide synthases encoded by B4galt5 and 6 genes are pivotal for neuronal generation and myelin formation in mice. *PLoS Genetics*, *14*, e1007545. https://doi.org/10.1371/journal.pgen.1007545

Yu, R. K., Tsai, Y. T., Ariga, T., & Yanagisawa, M. (2011). Structures, biosynthesis, and functions of gangliosides–an overview. *Journal of Oleo Science*, *60*, 537–544. https://doi.org/10.5650/jos.60.537

SUPPORTING INFORMATION

Additional supporting information may be found online in the Supporting Information section.

How to cite this article: McGonigal R, Barrie JA, Yao D, Black L, McLaughlin M, Willison HJ. Neuronally expressed a-series gangliosides are sufficient to prevent the lethal age-dependent phenotype in GM3-only expressing mice. *J Neurochem*. 2021;158:217–232. https://doi.org/10.1111/jnc.15365